Deutsches Elektronen-Synchrotron
and
Moscow Institute of Physics and Technology

Summer Student project

Studies of the CMS pixel detector

in the DESY testbeam using the Datura beam telescope

Author:
Mikhail Mikhasenko

Supervisors:
Daniel Pitzl
Hanno Perrey
Thomas Eichhorn

September 5, 2012

Acknowledgement

First of all, I would like to thank my supervisors, who made my summer useful and interesting. Daniel Pitzl for the motivation and good personal example, Hanno Perrey for my technical improvement and Thomas Eichhorn for the detail work with me. They were the best supervisors and I enjoyed my work.

Although, I want to thank my colleague Shiraz Habib who share room with my for company and help.

Thank Olaf Behnke and the Organizers of 2012 DESY Summer Student Program for wonderful summer and this possibility.

Contents

Chapter 1

Introduction and Motivation

1.1 The General CMS

The Compact Muon Solenoid (CMS) experiment is one of two large general-purpose particle physics detectors built on the proton-proton Large Hadron Collider (LHC) at CERN in Switzerland and France.

1.2 CMS pixel detector

In the center of CMS is the pixel tracking system. There are approximately 66 million pixels in the system.

Pixel modules are the main building blocks of the CMS pixel detector. The three barrel layers consist of 672 such modules and 96 half-modules at the edges of half cylinders. The modules are mounted on a structure of aluminum cooling tubes and carbon fiber blades which ensure low material budget. The radii of subsequent layers are 4.4, 7.3 and 10.2 cm. This allows for a high precision in track reconstruction but also causes large radiation exposure.

The pixel detector was installed into CMS in 2008, was commissioned with cosmic rays, and has been used to take collision data. The detector is performing well and meets design expectations.

1.2.1 Pixel chip module

A pixel detector module consists of the several layers. The sensitive part is the sensor which has 16 submodules of 4160 pixels, organized in 2 rows. Each submodule is split up on 52 columns and 80 rows.

The read-out chip (ROCs) is bump-bonded to sensor. The infrastructure (cables, mechanical fixation, ..) is shown in fig. 1.1.

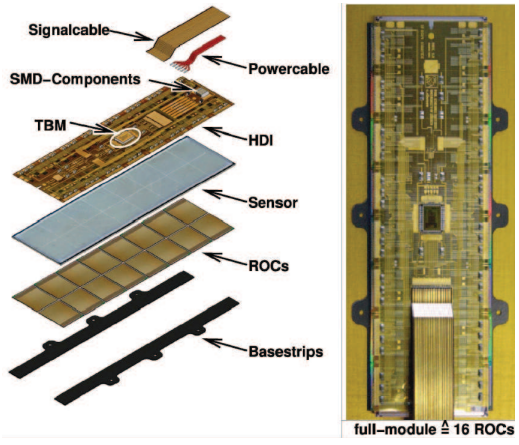

Figure 1.1: Physical processes in the CMS silicon sensor

1.2.2 Single chip

The 4160 pixels of a single chip are organized in 52 columns and 80 rows. The size of a pixel is $100 \times 150\,\mu\text{m}^2$ in the x-y direction and $285\,\mu$m in the z direction.

This size gives a high resolution for tracking in the 4 T magnetic field, because the Lorentz angle for electron drifting is 19°, that is angle of the best charge sharing between two pixels for that size. Thus this angle gives the highest resolution:

$$\alpha_{opt} = \arctan \frac{100\,\mu m}{285\,\mu m} = 19.3^\circ$$

That result was tested experimentally (see section 2.3.1).

1.2.3 Underlying physics

The working principle of a Si-detector is shown in fig. 1.2

When a particle is passing through the silicon electrons and holes are generated. Due to magnetic field they start to drift is silicon. The drifting velocity is proportional to the electric field. At CMS detector, drift occurs with angle according electric field lines, because of the magnetic field. That angle is called "Lorentz angle" and equals: $\alpha = \arctan(\mu B)$, here μ is a mobility of charge carriers, B is the magnitude of the magnetic field.

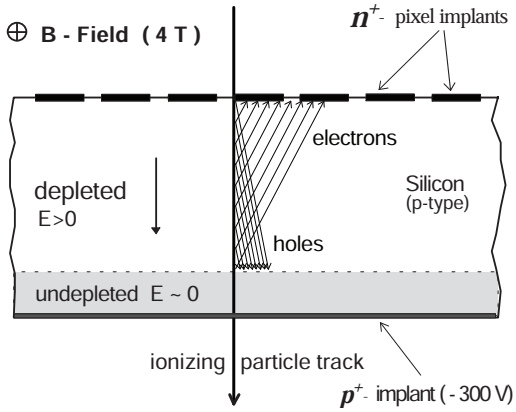

Figure 1.2: Physical processes in the CMS silicon sensor

1.2.4 Pixel chip readout and timing at testbeam experiment

Since the LHC design bunch crossing frequency is 40 MHz, the interval between bunch crossings is 25 ns which becomes a natural unit for data acquisition timing.

For CMS read-out chip to work correctly the clock (CLK) and trigger signals are required. The trigger signal is provided by a TLU system. The clock is generated based on the DESY-II revolution signal. This signal is going to the pulse generator, which produces 39 pulses with a frequency $\frac{1}{24.3\,ns} =$ 41 MHz. The chapter 3 is dedicated to several clock-trigger timing studies.

A single front-end cell scheme is shown in fig. 1.3.

When electrons and holes are drifting, they are generated a current pulse which is directed into a preamplifier and shaper and further into a comparator.

The read-out chip has three modification. The difference between generations you can see in table.

generation	sensor-chip	chip-board	output	additional feature
psi46	analog	analog	digit	
xdb	analog	analog	digit	extended buffer
digi	analog	digi	digit	ADC was moved to sensor electronics

A signal from each pixel is compared to the threshold in the comparator and further stored into a sample-and-hold capacitor. The dependencies of signals from threshold were studied. That analysis is being discussing in section 2.3.2.

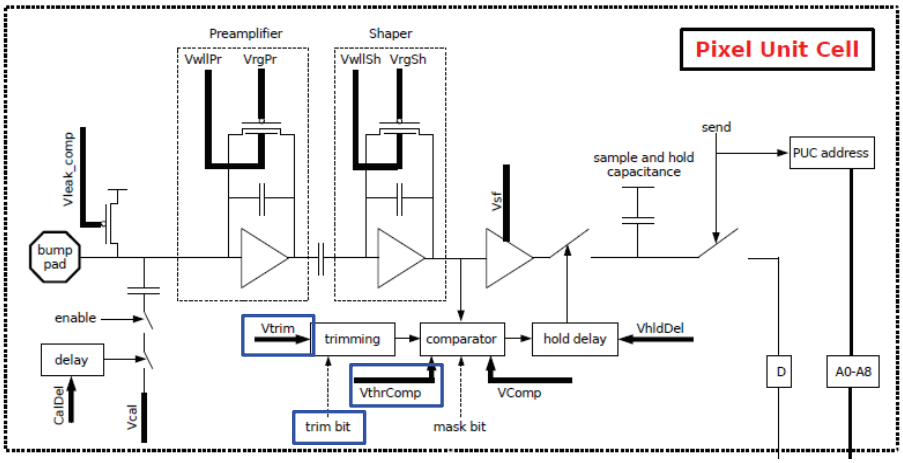

Figure 1.3: Physical processes in the CMS silicon sensor

1.3 Testbeam

For the testbeam a bremsstrahlung radiation beam from DESY-II synchrotron was used. The principle of the testbeam generation is shown in fig. 1.4 The bremsstrahlung radiation is generated by a carbon

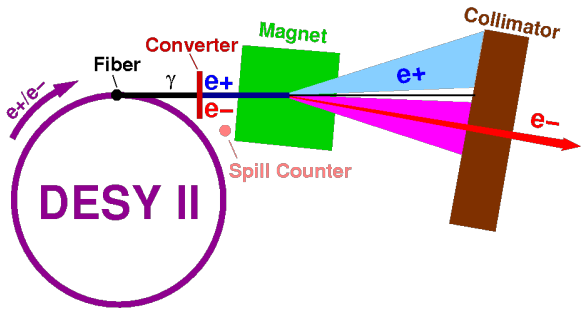

Figure 1.4: Pixel charge distribution for run 3633

fiber in the circulating beam and hits a copper target to create $e^+ e^-$ pairs. The positrons/electrons of the desired energy are then selected from the secondary beam with a magnetic field. Like a slice, the final beam is cut out of this fan with a collimator.

1.3.1 Beam structure

The frequency of DESY-II is approximately 1.024 MHz. It means that the time interval between particles should be a multiple of DESY-II cycles. That principle was used for trigger and clock analysis (see chapter 3). But not only the DESY-II revolution frequency determines time structure of incoming particles, as there is an energy cycle with a period of 80 ms. This corresponds to 12.5 Hz. The beam energy is changing as shown in fig. 1.5a

Obviously, we have particles of the specified energy in the testbeam only if the beam energy in the DESY-II is higher. Also the average rate of particles depends on the energy (see fig. 1.5b).

The injection from the linear accelerator into DESY occurs every 320 ms. Moreover, the electron/positron synchrotron DESY-II is mainly an injector for DORIS and PETRA. Typically, when running in PETRA mode, DESY-II injects particles every minute to PETRA. This process takes about $2 - 6$s.

1.3.2 Datura Pixel Telescope

Track reconstruction can be performed with the Datura pixel telescope. The Datura telescope (see fig. 1.6) is a special detector which provides a flexible and portable infrastructure in order to be able to investigate quite different devices-under-test (DUT). It consists of two arms: for incoming track and out-coming one. The system of sensors is called Mimosa 26. Each arm equipped with three sensors kept at a stable temperature by a cooling system. The resolution of the telescope is 5.5 μm.

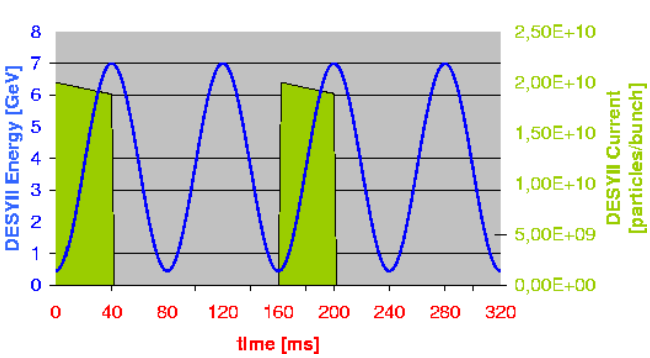

(a) Ideal DESY-II energy cycle

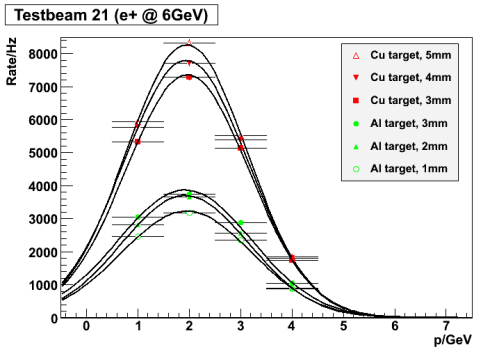

(b) Rate vs beam energy for Testbeam 21: about $7 * 10^9$ positrons @ 6 GeV, more than one carbon wire, different targets

Figure 1.5: DESY-II cycle and particle rate at channel 21

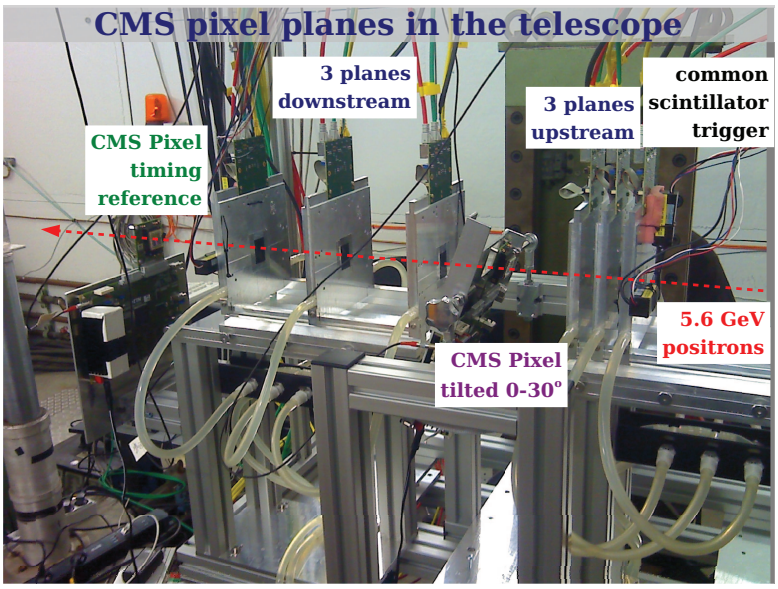

Figure 1.6: The Datura telescope installed at the 21 channel DESY

Particle track information was used for resolution and efficiency measurements. These measurements will be described below.

For the CMS chip to be triggered, the telescope Trigger Logic Unit (TLU) is used. The trigger system includes four scintillators connected to photomultiplier tubes, allowing triggering on particles passing through the telescope.

1.3.3 Setup

The scheme of the experimental setup is shown in fig. 1.7

The upstream arm planes $(0 - 1 - 2)$ of the telescope serve for tracking purposes in front of the DUT. They are set as close as possible to the CMS chip to improve the quality of tracking.

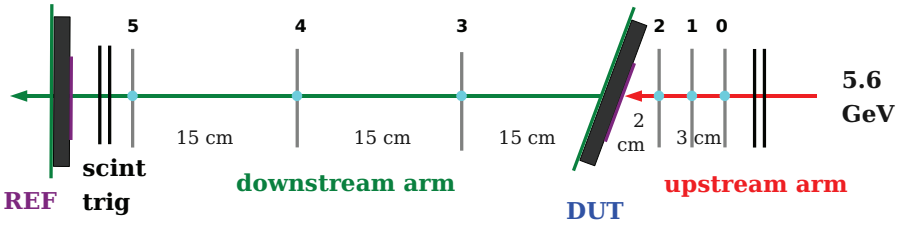

Figure 1.7: Schematic of experimental set up

The mechanical fixation of the DUT provides possibility to do measurements with different tilts from 0 to 30 deg.

Chapter 2

Measurements

This chapter will describe the measurements taken and the theoretical background.

2.1 Single pixel studies

For each pixel the deposited charge is measured. A typical pixel charge distribution is shown in fig. 2.1 It is very interesting to give a theoretical estimation for the shape of the pixel charge distribution.

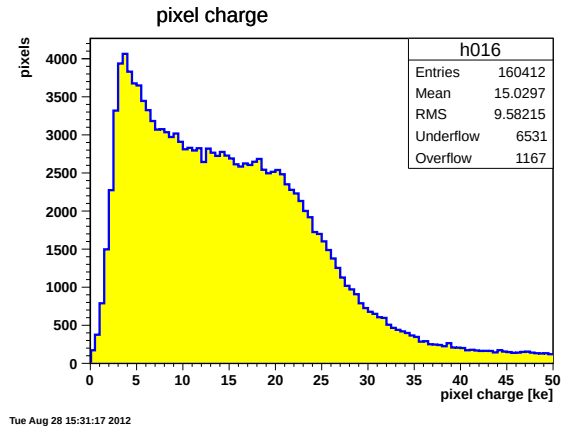

Figure 2.1: A typical pixel charge distribution, measured in the run 3633

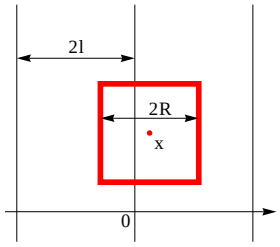

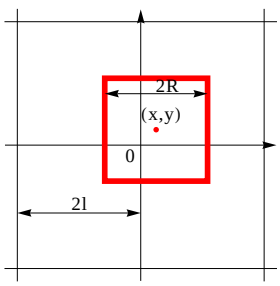

My calculation for the probability distribution for a pixel charge is based on the simplification that the shape of the "diffusion" area is a square with the side R and that the charge is distributed evenly. The side of pixel is l. To derive the pixel charge distribution we can calculate the probability distribution function under our simplification and then convolute it with the Landau distribution. This is because the charge of the "diffusion" rectangle is described by a Landau function.

In one dimension this is trivial but doesn't explain shape of the the pixel charge distribution. This function is described by a formula and shown in fig. 2.3a

$$\rho(A) = \frac{1}{2l}[1 + 2(1 - R)\delta(a - 2R)],$$

here $A \leq 2R$.

Let's follow to $2D$ model. $(x; y)$ is the coordinates of the center of the "diffusion" square. If $|x| < l - R$ and $|y| < l - R$ the whole area is situated in one pixel; in the opposite case our measured charge is proportional geometrical cross section (A) of the "diffusion" square and the pixel area. The variety of the center points, which corresponds the same A is called equipotential line (fig. 2.2a). To construct the probability distribution function

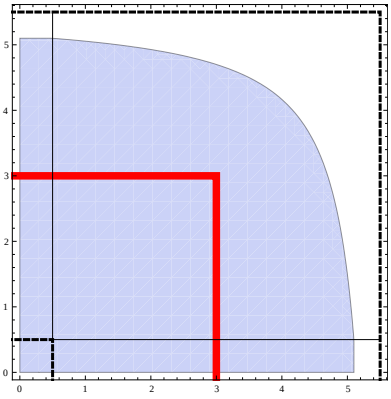

(a) The blue area (S) is calculated, the dashed lines are restrictions $l + R$ and $l - R$

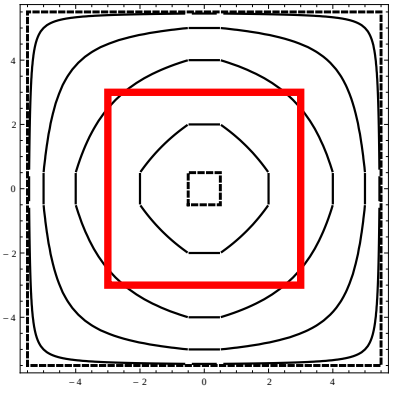

(b) The equipotential lines are black ones

Figure 2.2: A quarter of a pixel: the red line is the boundary of the pixel. Here $l = 3$, $R = 2.5$

($\rho(A)$) for A we should calculate the area between two equipotential lines for A and $A + dA$. They should be equal to $\rho(A)dA$.

For $x > l - R$ and $y > l - R$ equipotential lines are

$$A = (l + R - x)(l + R - y), \qquad y(x) = l + R - \frac{A}{l + R - x}$$

Calculate the whole area inside one equipotential line (fig. 2.2b):

$$S = 4\left[(l - R)^2 + (l - R)(2R - \frac{A}{2R}) + \int_{l-R}^{l+R-\frac{A}{2R}} y(x)dx\right] =$$

$$= 4\left[(l - R)^2 + (l - R)(2R - \frac{A}{2R}) + \frac{l + R}{2R}[4R^2 - A] + A \ln \frac{A}{4R^2}\right]$$

The differential area between A and $A + dA$ equals dS.

$$dS = -4\left[\frac{l - R}{2R} + \frac{l + R}{2R} - \ln \frac{A}{4R^2} - 1\right] dA$$

$$dS = -4\left[\frac{l - R}{R} - \ln \frac{A}{4R^2}\right] dA$$

As a result we have the probability distribution function normed by 1. The graph is shown in fig. 2.3b

$$\rho(A) = \frac{1}{(l + R)^2}\left[\frac{l - R}{R} - \ln \frac{A}{4R^2} + (l - R)^2\delta(A - 4R^2)\right]$$

Now we need to convolute this distribution (see in fig. 2.3b) with the Landau distribution. The final result isn't shown, but we expect that it confirms experimental data.

2.2 Cluster studies

A cluster is defined as a group of pixels which have a non-zero signal and share an edge. The size of a cluster depends on the angle and the coordinate of the passing particle. A typical histogram of the cluster size is shown in fig. 2.4a. We can see that the average size of a cluster equals 2.05 pixels.

Important cluster characteristics are the number of columns and rows per cluster, because they give information on the angle of the particle and allow to evaluate the hit point very precisely.

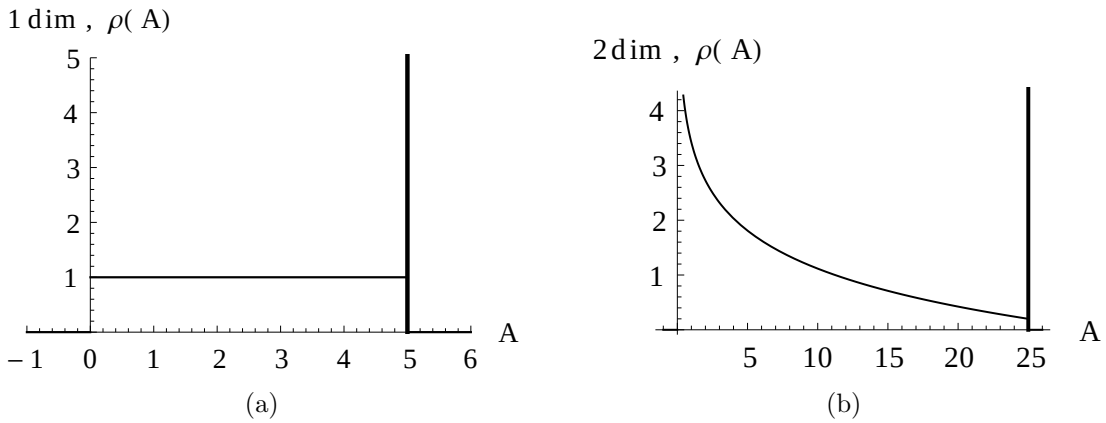

(a) (b)

Figure 2.3

2.2.1 Cluster charge

The charge of a cluster (it will be called CC later) is defined as the charge sum of all consisting pixels. The value of the cluster charge should be the corresponding energy loss of the particle. In our experiments a typical energy for the electrons was in the range of $4.8 - 5.6$ GeV. An electron with that energy is a Minimal Ionizing Particle (MIP). A distribution of energy loss for MIPs is the Landau distribution. We can see in fig. 2.4b that the measured distribution corresponds to the expected one. The most informative value of a cluster charge distribution is the position of the peak because it corresponds to the deposited energy. The histogram is fitted by a landau convoluted with gauss function to take peak value. The Gaussian function is needed to account for a noise and non-uniformities.

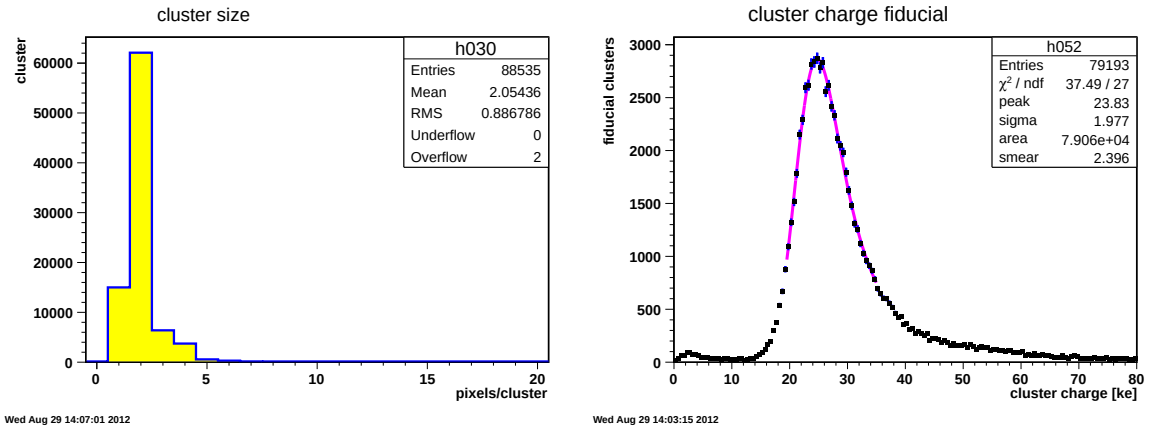

(a) A cluster size distribution (b) A cluster charge distribution

Figure 2.4: typical distribution for clusters

2.2.2 Efficiency and resolution

The next step of data processing is an efficiency measurement. The Mimosa sensors allow us to reconstruct tracks of particles, and interpolate them to the CMS chip. The comparison coordinates of the interpolation and the CMS signal coordinates gives us information about precision and the efficiency of the CMS pixel detector. The efficiency is calculated by

$$\varepsilon = \frac{N_{cms}}{N_{mimosa}},$$

The efficiency should be very high, at approximately $99,86\%$. Moreover, it was calculated for each pixel and as a function of time, these plots are shown below.

The resolution is the distance between the track interpolation point and the CMS signal coordinate. That distribution for measured distance value is shown in fig. 2.5c, where we can see that the width

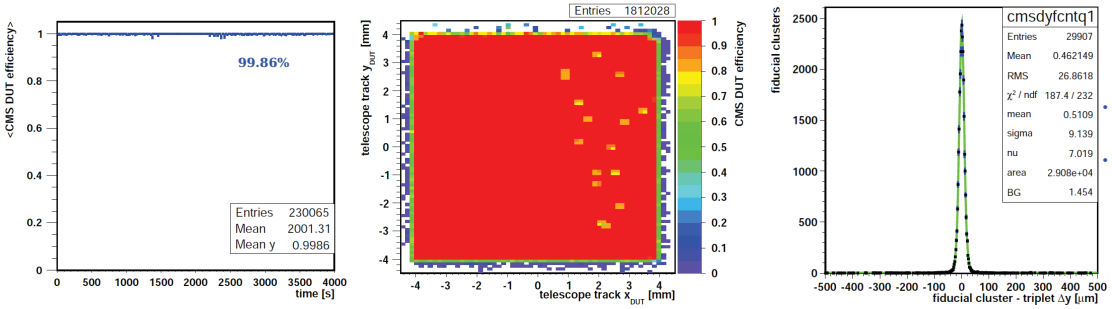

(a) Efficiency of the CMS chip vs time (b) The map of efficiency for the CMS chip (c) a typical resolution plot

Figure 2.5: Efficiency and resolution

of this distribution is 9.1 μm. The resolution of the Datura telescope is 5.5 μm, so the resolution for the CMS pixel detector (DUT):

$$\sigma^2_{measured} = \sigma^2_{DUT} + \sigma^2_{telescope}, \qquad \sigma_{DUT} = 7.4\,\mu m$$

2.3 Measurements as function of angle, thresold and bias

A wide range of important measurements were made. To study the characteristics of the CMS pixel detector with a different geometry a cluster charge, cluster size, resolution, efficiency is measured as a function of the angle to the beam.

The threshold scan emulate the radiation damage. Bias voltage scans allow to determine the depletion voltage range.

2.3.1 Angular measurements

A certain angle of the CMS chip was provided by mechanical fixation. Experimental settings are shown in fig. 2.6

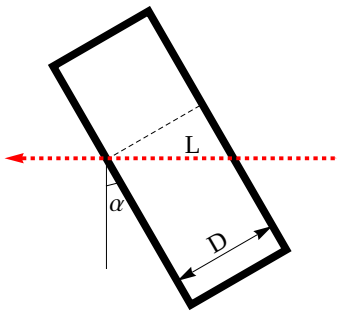

Figure 2.6: Schematic of experimental set up

We can see that the position of the Landau peak is changing, in other words the deposited energy in the pixel detector is changing. This effect is interpreted by geometry as well: the path of the particle in the substance is l, D is thickness of the chip and $l_\perp$ is the projection of the particle trajectory in the substance to the surface of the chip. The last value corresponds to the numbers of rows per cluster.

$$l = \frac{D}{\cos\alpha}, \qquad l_\perp = D\tan\alpha.$$

So the energy loss as well as cluster charge for a minimal ionizing particle (MIP) is linear function of $1/\cos\alpha$ (see fig. 2.7a).

Obviously row per cluster changing can be explained as well. This should be proportional $\tan\alpha$. That measurement is shown in fig. 2.7b

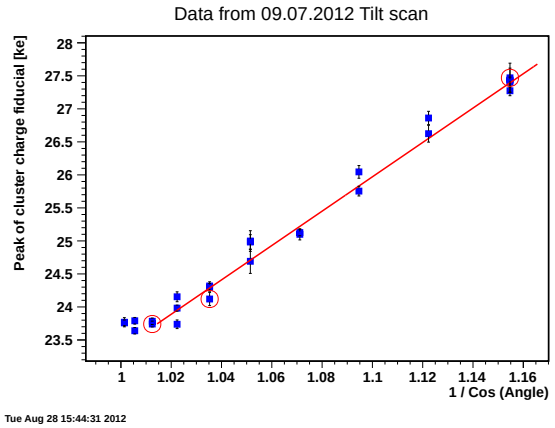

(a) A cluster charge as a function of $1/\cos\alpha$

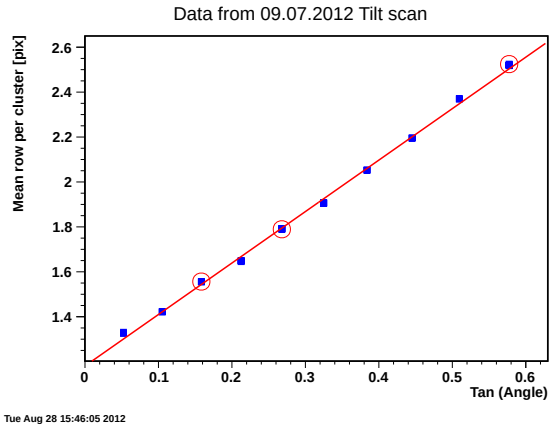

(b) A cluster size as a function of $\tan\alpha$

Figure 2.7: Cluster charge and a Cluster size as a function of the angle

2.3.2 Threshold dependency

The simplest result of the threshold influence we can notice in the pixel charge distribution.

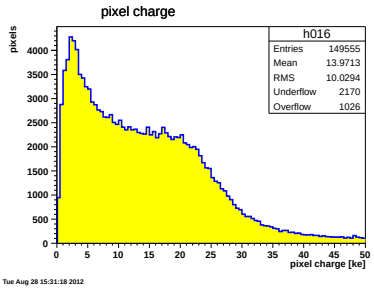

(a) the threshold 1.6 keV

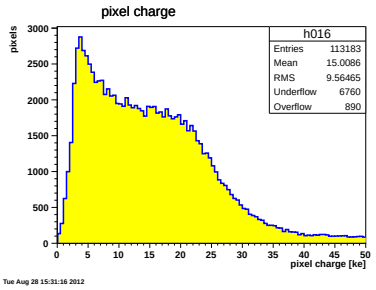

(b) the threshold 2.7 keV

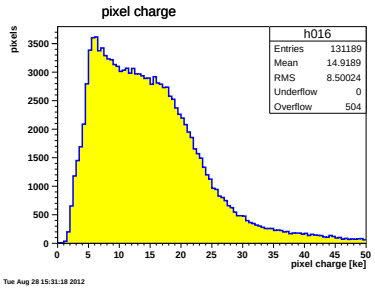

(c) the threshold 5.4 keV

Figure 2.8: Pixel charge plot under different threshold values

To give an explanation to the results is more complicated than in the previous case. Let's consider simple model.

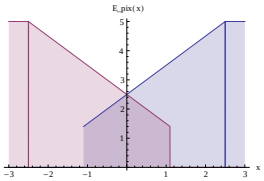

Figure 2.9: The energy deposit per one pixel as a function of the coordinate. x is coordinate of the center of the "diffusion" square. If $-R < x < R$, then the energy loss is split between several pixels. The influence if threshold is shown. In the energy deposit is less then $T = 1.4$ the signal is lost.

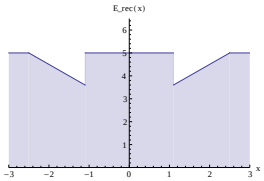

Figure 2.10: The sum of energy of two neighboring pixels as a function of the coordinate. The amplitude is $A = 5$. The signal is less than the threshold ($T = 1.4$) in one of the pixels, is the reason for a loss in the sum of the signals.

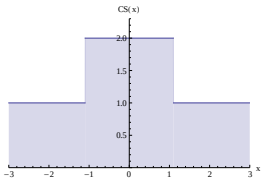

Figure 2.11: The size of a cluster as a function of the coordinate. The coordinate interval for cluster size equaled 2 depends on threshold (T).

Assume that the "diffusion" area is a square with face R. When a particle is passing through to the pixel far from the boundary, all of the energy is lost in the pixel. If a particle is passing through

the pixel near neighboring ones, the energy loss is split between several pixels. So the energy for one pixel as a function of coordinate of center of the "diffusion" square should look like trapeze (fig. 2.9). A signal threshold cuts into this distribution at small values. In this situation we have a loss of signal. Reconstructed energy(E_{rec}) as a function of hit point coordinate is shown in fig. 2.10 The average value of reconstructed energy might be calculated:

$$\bar{E}_{rec} = \frac{1}{2l}\int_{-l}^{l} E_{rec}(x)dx = E_0(1 - \frac{R}{l}\frac{T^2}{E_0^2}),$$

Here T is the value of the threshold, E_0 is the energy loss of the particle and the side of pixel is R.

The amount of pixels per cluster as a function of the hit coordinate is shown in fig. 2.11 The averaging procedure gives:

$$\bar{CS} = \frac{1}{2l}\int_{-l}^{l} CS(x)dx =$$

$$= \frac{1}{2l}\left[1 \times (2l - 2(R - R\frac{2T}{A})) + 2 \times 2(R - R\frac{2T}{A})\right] = 1 + \frac{R}{l} - \frac{R}{l}\frac{2T}{A}$$

It is worth emphasizing, that $\bar{E}_{rec}$ is a parabolic function of the threshold(T), $\bar{CS}$ is a linear function of T.

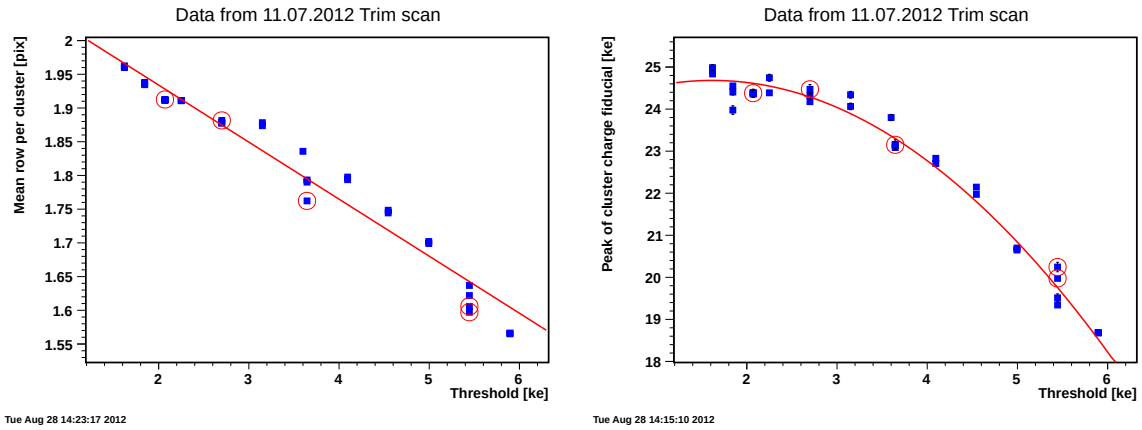

(a) CS as function of the threshold (b) CC as function of the threshold

Figure 2.12: Cluster charge and a cluster size as a function of the threshold

Below we will discuss the coordinate resolution of chip as a function of threshold.

If the threshold is small enough and most clusters consist of two or more pixels, a measurement of coordinates can be performed very precisely. This behavior is observed at the experiment (fig. 2.13a).

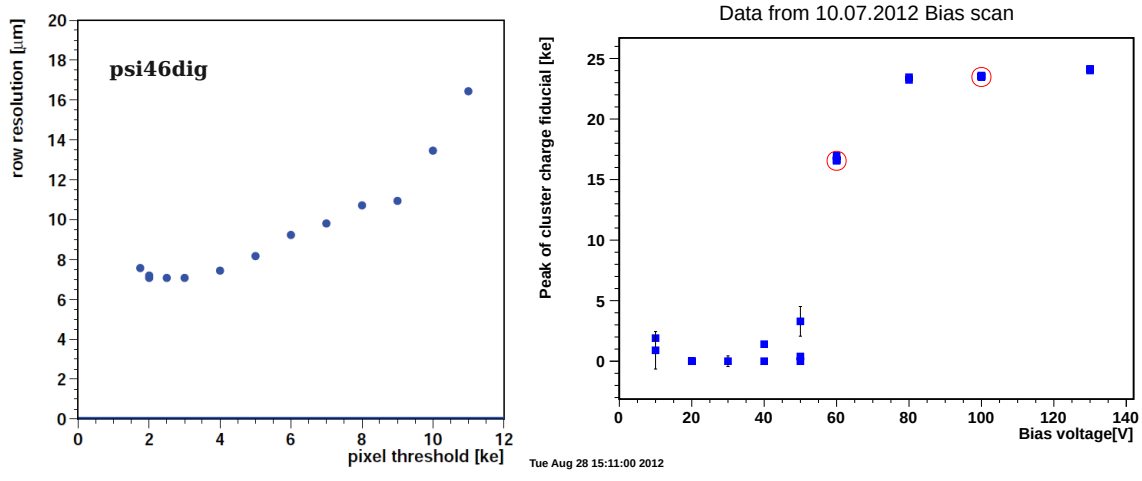

(a) Resolution as function of the threshold (b) CC as function of bias voltage

Figure 2.13

2.3.3 Bias measurements

For the bias measurement, we can see that the chip doesn't work with a bias voltage less than 50 V. The stable working condition can be expected with a bias voltage of more than 80 V. Rough approximation gives 75 V for the depletion voltage.

Chapter 3

Trigger and Clock studies

3.1 Motivation

We had runs is which the efficiency wasn't stable during the run time (see fig. 3.1). Drops in efficiency were from 10% to 90%. The investigation of possible reasons of the drop is described in this chapter.

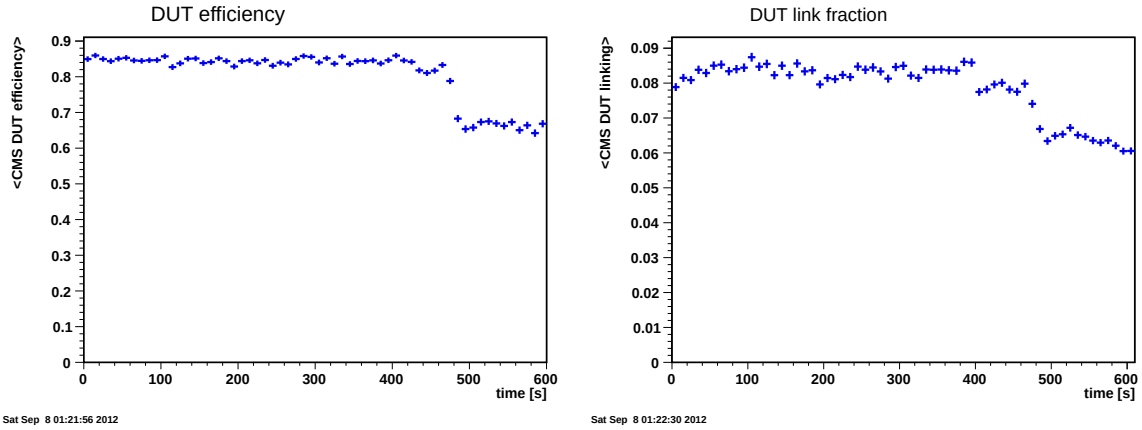

(a) typical yield drop

(b) typical efficiency drop

Figure 3.1: The drop in efficiency and yield, telescope run 4757

3.2 Method of analysis

The DESY-II frequency is 1.024 MHz, which is equal to the length of the DESY-II beam pipe divided by the speed of light. The internal TLU clock runs at approximately 384 MHz, it specifies the accuracy of our trigger signal. The information about the time interval between triggers can give us information about the beam structure and even small changes and delays. The convenient way to work with timing is to use modulo-operator. It was mentioned before that a difference between triggers should be a multiple of the DESY-II cycle. One circle of the particles in DESY corresponds roughly to 384./1.024 = 375. clocks of TLU. Here and below the point after value (for instance 375.) means the value has a fractional part. If this value is estimated precisely, a remainder after modulo-operation should be zero.

For our studies it is very comfortable to use special units called that "trigger units". The idea is to define TLU clock frequency as $1\,\frac{1}{clk}$, so the time for the particle circle is about 375. clk. The dependency is mentioned in table.

	particles	TLU
normal units		
f	1.024 MHz	386. MHz
τ	$\frac{10^{-6}}{1.024}$ s $\approx 1\,\mu$s	$\frac{10^{-6}}{386}$ s ≈ 2.6 ns
"trigger units"		
f	$\frac{1}{375.}$ clk^{-1}	1 clk^{-1}
τ	375. clk	1 clk

This basic idea is applied to the CMS time studies as well. For CMS we have 39 clocks per particle turn in DESY-II. A remainder after modulo-operator for DESY time interval, counting in DESY clocks has to be zero.

The histogram "difftime mod" shows a rest after the modulo-operation for revolution time in the DESY-II.

The "time structure" serves to detect time shifting between triggers. A remainder after the modulo-procedure for absolute time is histogramed. The most instructive way is to see this plot versus time.

3.3 The TLU analysis

A time difference between particle triggers variates a lot, from $10^{2.6}$ clk $\approx 8\,\mu$s to $10^{7.5}$ clk $\approx 80\,m$s, according to fig. 3.2

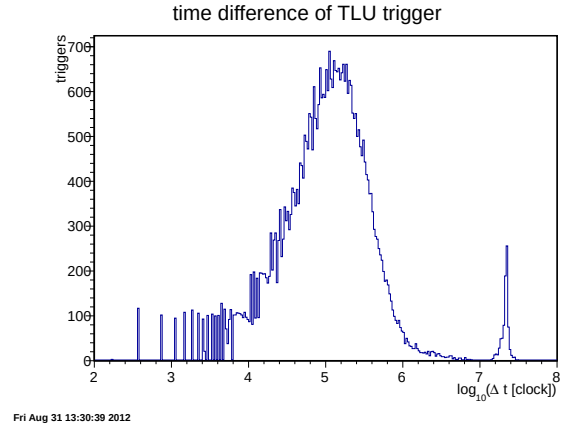

Figure 3.2: A time difference between particle triggers in log-scale

3.3.1 The revolution time measurement

To evaluate revolution frequency a scan was made. The plot "difftime mod" was created for different values modulo-denominator. If the value is correct, all time differences give about 0 as a remainder after modulo-operation.

Let us consider the last approximation in detail. We can see in fig. 3.3d two crossed lines. Our frequency spectrum (fig.) is quite wide, so when the time value, which is measured in this scan, isn't correct, it is a low frequency, which indicates the error, because the during long time distance between triggers particles do many turns and the errors of scanned time value is accumulate. To illustrate it I want to give one example:

τ is the correct time difference for the particle revolution,
T is time difference for one frequency in the spectrum. $T = n \cdot \tau$, here n is the multiplicity of the frequency. The scan parameter is x.

$$T\ mod\ x = \frac{n\tau}{\tau + \Delta x} = \frac{n(\tau + \Delta x) - n \cdot \Delta x}{\tau + \Delta x} = -n \cdot \Delta x = const - n \cdot x$$

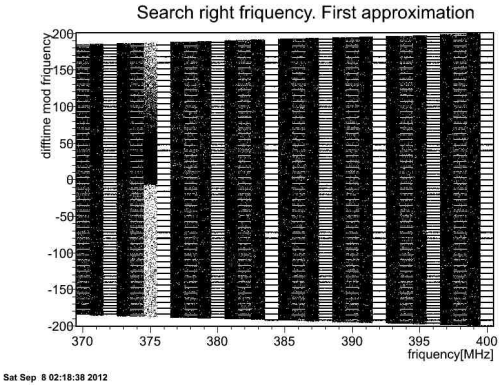

(a) the first approximation

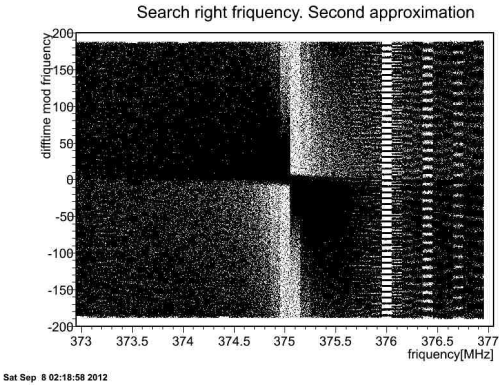

(b) the second approximation

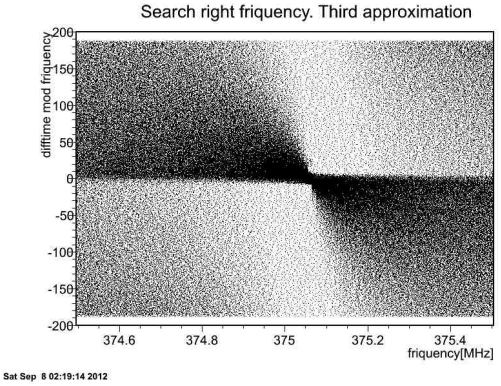

(c) the third approximation

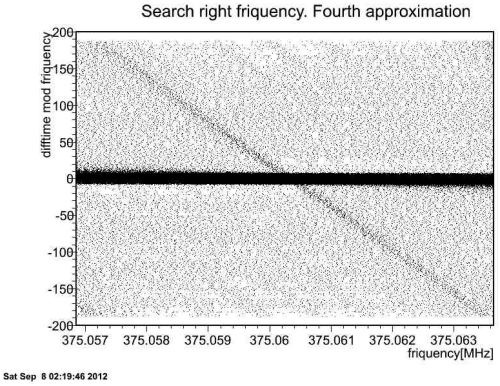

(d) the fourth approximation

Figure 3.3: The particles circle frequency scan

The measurement of the slope gives $n \approx 8 \cdot 10^4$. It is $\frac{10^6}{8 \cdot 10^4} = 12.5\,\text{MHz}$ in normal units, which is the energy-cycle of DESY. It is worth mentioning that we can see energy cycle frequency peak in fig. 3.2

The revolution time was measured by 375.060423 for considered run.

3.3.2 A changing of the revolution time

We know the DESY-II revolution time very precisely. Now let's consider the "time structure" plot versus time. The different scales of this plot are shown in fig.

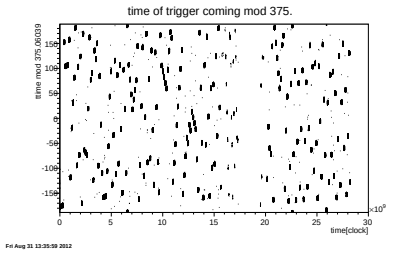

(a) 30 s

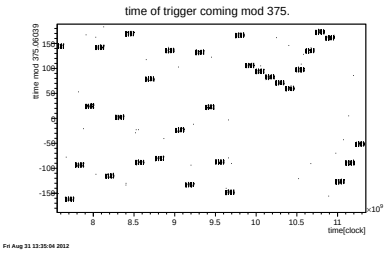

(b) zoom 15 s

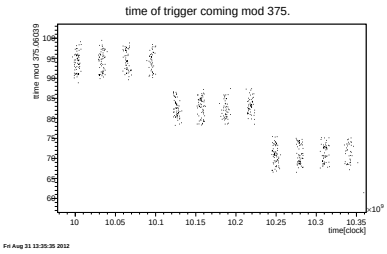

(c) zoom 1.2 s

Figure 3.4: The different scales for "time structure" plot

We can see a lot of "strip" following one by one. The time length of each strip is 0.3 s. The vertical shifting means the time interval between triggers has a remainder after the modulo-operation. There aren't shifts inside a strip, but an each one is shifted compared to the previous. The strip is portion of the particle in DESY-II. An new injection is started independently and the shifts are arbitrary. I won't pay attention on this shifting. (I tried to cut that interval and see the slow changing, may be I catch to show this plot).

The accuracy of the time interval turning is **six** digits after point for time interval in clocks. This result looks strange from naive point of view.

But it is explained very good precision of the accelerator between the injections. The time between injections is 0.3 s, so we have approximately 3×10^5 cycles for particles. The frequency is wrong the strip on the time structure plot has slope corresponding frequency error. The slope in one clock during 0.3 s is

$$\Delta\tau = \frac{1\,clk}{0.3 \cdot 10^5} = \frac{1}{3 \cdot 10^5}\,clk = 3 \cdot 10^{-6} clk$$

$$\Delta\tau = 3 \cdot 10^{-6} clk \approx 9 \cdot 10^{-15} = 9\,fs$$

The accuracy of the accelerator is impressive, indeed. But the turn frequency isn't constant. It is changing from one run to other. My evaluation for different runs you can see on the table below. The changing of DESY-II revolution frequency is measured according to $\tau_0 = 375.060000$

run number	date-time	timing [clk]	$\Delta\tau_0 \times 10^6$ clk	$\Delta R\,[\mu$m]
4748	54.54.12	375.060065	65	9
4751	54.54.12	375.060065	65	9
4757	54.54.12	375.060035	35	5
4762	54.54.12	375.060020	20	3
4763	54.54.12	375.060020	20	3
4764	54.54.12	375.060020	20	3
4766	54.54.12	375.060015	15	2
4769	54.54.12	375.060010	10	1.3
4772	54.54.12	375.060008	8	1
4774	54.54.12	375.060000	0	0
4780	54.54.12	375.059990	-10	-1.3

The possible reason of changing DESY-II revolution frequency is the changing of the radii of the particle orbit.

$$\Delta R = \frac{c\Delta t}{\pi}, \qquad \Delta R\,[\mu m] \approx 50\Delta t\,[ps]$$

3.4 The CMS analysis and the drop region

The similar analysis we did for the telescope trigger we can do using CMS information about time differences.

3.4.1 CMS only

The plot "difftime mod" was created for the CMS time differences between triggers. This measurement versus time is shown in fig. 3.5

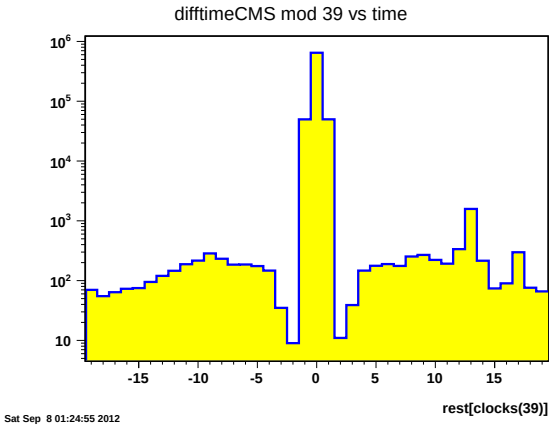

Figure 3.5: "difftime mod" for the CMS. Logarithmic scale

Several runs with the drop were studied. At the drop region the frequency was being changed. Instead of one line corresponding 39 clocks we have three. It could be solution of problem, but that effect doesn't cause the drop in the efficiency.

3.4.2 CMS vs TLU

The comparison of the CMS and TLU signal gives more information and increases precision. Let's imagine that the particle signal is changed, at the same time DESY-II signal is changing as well. The subtraction of the TLU and the CMS signals should give $0 \pm \frac{375}{39} \approx 9.5$. The function

$$dt(TLU) - \frac{375.}{39} \times dt(CMS) \, mod \, 375.$$

has to reduct the delays and shows relative shifting. This plot is shown in fig. 3.7a, 3.7b.

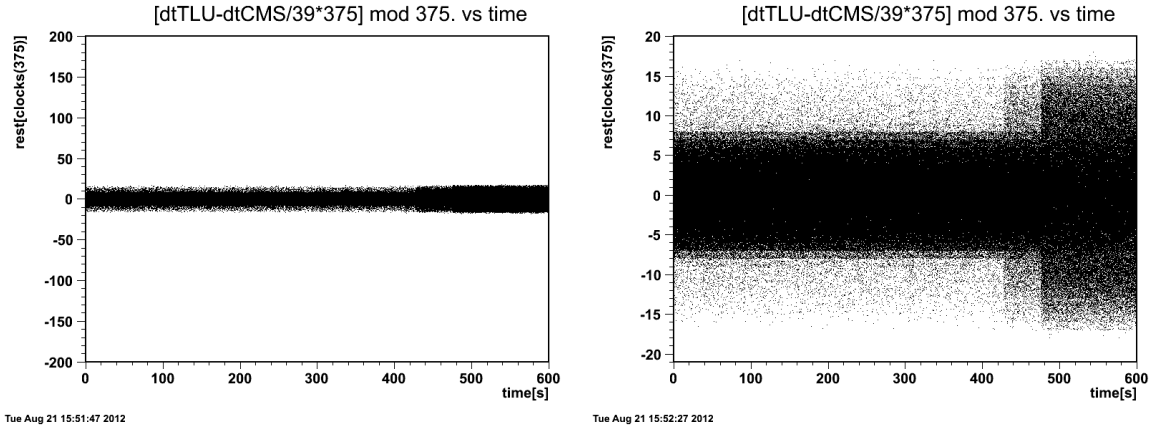

(a) the "difftime mod" vs time plot for the CMS, the band is uncertainty in DESY clock

(b) zoom Y. we can see drop region

Figure 3.6: difftime between triggers according to CMS in TLU clocks

We can see that in the drop region the width of the "difftime mod" vs time distribution is increasing. It is worth comparing this distribution and the same "difftime mod" vs time distribution for TLU only.

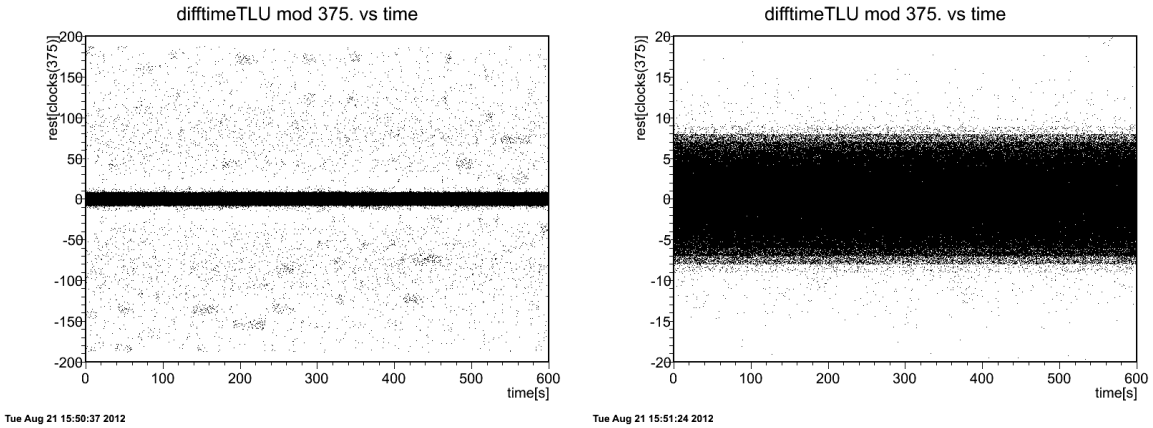

(a) the "difftime mod" vs time plot for the TLU signal

(b) zoom Y. we can see drop region

Figure 3.7: difftime between triggers according to TLU

There aren't any visible changes of TLU signal in drop region. It means the trigger signal for read-out board is fine. We should find the problem with clock or instability of board electronics.

Chapter 4

Conclusion

First part of the work was dedicated to measurement of characteristics of CMS pixel detector. We use Datura telescope to have "well-defined" track and calculate efficiency and resolution.

The angle-, threshold-dependencies of the resolution were studied. The bias voltage scan had given the depletion value equaled 75 V.

The theoretical predictions were derived and confirmed with experiment.

To draw conclusion I want to emphasize important results for CMS pixel detector studies:

1. analyzed chip works well
2. the behavior under radiation damage is predicted and expectable.
3. feedback to chip designer was given

The second part was about timing studies. The general results based our analysis is listed below:

1. approach for a timing analysis was developed and the DESY revolution frequency was maesured using that.
2. changes of DESY-II revolution signal were detected
3. efficiency drops can be linked with clock timing.
4. same plots can help to identify runs with timing problems.